http://dx.doi.org/10.5516/NET.01.2014.066

COARSE MESH FINITE DIFFERENCE ACCELERATION OF DISCRETE ORDINATE NEUTRON TRANSPORT CALCULATION EMPLOYING DISCONTINUOUS FINITE ELEMENT METHOD

DONG WOOK LEE and HAN GYU JOO*
Department of Nuclear Engineering, Seoul National University
1 Gwanak-ro, Gwanak-gu, Seoul, 151-744, Korea
*Corresponding author. E-mail : joohan@snu.ac.kr

Received June 10, 2014
Accepted for Publication July 29, 2014

The coarse mesh finite difference (CMFD) method is applied to the discontinuous finite element method based discrete ordinate calculation for source convergence acceleration. The three-dimensional (3-D) DFEM-Sn code FEDONA is developed for general geometry applications as a framework for the CMFD implementation. Detailed methods for applying the CMFD acceleration are established, such as the method to acquire the coarse mesh flux and current by combining unstructured tetrahedron elements to rectangular coarse mesh geometry, and the alternating calculation method to exchange the updated flux information between the CMFD and DFEM-Sn. The partial current based CMFD (p-CMFD) is also implemented for comparison of the acceleration performance. The modified p-CMFD method is proposed to correct the weakness of the original p-CMFD formulation. The performance of CMFD acceleration is examined first for simple two-dimensional multigroup problems to investigate the effect of the problem and coarse mesh sizes. It is shown that smaller coarse meshes are more effective in the CMFD acceleration and the modified p-CMFD has similar effectiveness as the standard CMFD. The effectiveness of CMFD acceleration is then assessed for three-dimensional benchmark problems such as the IAEA (International Atomic Energy Agency) and C5G7MOX problems. It is demonstrated that a sufficiently converged solution is obtained within 7 outer iterations which would require 175 iterations with the normal DFEM-Sn calculations for the IAEA problem. It is claimed that the CMFD accelerated DFEM-Sn method can be effectively used in the practical eigenvalue calculations involving general geometries.

KEYWORDS : DFEM, Sn Method, Source Convergence Acceleration, General Geometry Application, Partial Current Based CMFD

1. INTRODUCTION

For the analysis of fast neutron systems including complicated structures such as fast liquid metal cooled reactors or fusion breeding blankets, a general geometry neutron transport code capable of handling unstructured meshes is required. The solution of the neutron transport equation on unstructured meshes is usually obtained by employing the finite element method (FEM) to solve the discrete ordinate (Sn) equation. The ATTILA [1,2] and MUST [3] codes employed the discontinuous finite element method (DFEM) [4,5] for a practical realization of FEM-Sn. DFEM, that was first introduced by Reed and Hill [4] and recently reviewed thoroughly by Cockburn et al. [5], permits relaxed continuity of the physical quantities at the inter-element boundaries; although, continuity is eventually satisfied as the iterative solution converges. The advantage of this method is the possibility of decoupling local problems from the global one. Namely, it is possible to construct a set of small linear systems satisfying the governing equation for each element to avoid assembling and solving the global linear system.

For the application of a transport code to large reactor problems, an efficient acceleration method is essential because a significant number of fission source iterations are required in solving the eigenvalue problems that involve large dominance ratios. As one of the fission source acceleration methods, the coarse mesh finite difference (CMFD) method [6] has been widely used in various types of core calculations owing to its efficiency and versatility. It was originally applied to the nodal diffusion methods, but it was later extended to various transport calculations: the method of characteristics (MOC) transport calculations [7,8], the discrete ordinate Sn transport calculations [9,10] and the Monte Carlo calculations [11]. Remarkable

reduction in the number of fission source iterations was reported with the CMFD formulation. Particularly, it was observed that acceleration performance increases significantly as the core size increases [12].

Traditionally the diffusion synthetic acceleration (DSA) method [13] had been used to accelerate Sn calculations [14,15,16]. Degraded effectiveness of the DSA method was, however, observed under the presence of material discontinuities in multidimensional problems [17]. As an alternative of the DSA method, the CMFD method was applied first to the NEWT two-dimensional (2-D) Sn lattice physics code for both regular and irregular coarse mesh geometries [9,10]. The acceleration performance of CMFD-Sn, however, turned out to be deficient for the 2-D lattice problems because the dominance ratio of the lattice problems is not large. For the three-dimensional (3-D) larger core problems, it is expected that the acceleration gain by the CMFD formulation for Sn calculations would be considerably large. This expectation provides the basic motivation for this work. The implementation of the CMFD formulation to the DFEM-Sn solution process however poses a nontrivial problem because the angular fluxes resulting from the DFEM-Sn calculation are not continuous at the interface points from which the net currents are to be obtained. Note that the net current of the transport calculation is used to determine the current correction coefficient of the CMFD relation between the interface net current and mesh average fluxes. In this regard, several methods are devised and investigated in this work; including the partial current based CMFD method [18].

The CMFD acceleration methods are implemented into a 3-D DFEM-Sn code named FEDONA (Finite Element Discrete Ordinate Neutronic Analysis) that employs unstructured tetrahedron linear elements to obtain the DFEM solution of the Sn equation. The meshes are generated by a public mesh generation utility Gmsh [19]. FEDONA has the capability to solve eigenvalue problems as well as fixed source problems containing complicated pin cells or fuel assemblies without homogenization. The basic formulation and key features of the code are presented first in Section 2.

In order to establish CMFD acceleration of DFEM-Sn calculations, the following problems have to be resolved: 1) formulation of coarse meshes by combining tetrahedron finite elements, 2) acquisition of coarse mesh averaged fluxes, 3) determination of the coarse mesh surface current considering the discontinuity of angular fluxes at the interface of two elements, and 4) securing convergence stability of the acceleration scheme. In particular, the problem of convergence stability in the CMFD acceleration of high order methods needs special attention. As reported by the several Fourier convergence analysis of the CMFD acceleration for eigenvalue problems [20,21,22], the spectral radius of the CMFD iteration matrix is strongly affected by the coarse mesh size and divergence can occur for larger CMFD meshes. As an effort to improve the convergence of CMFD for larger meshes, the partial-current based CMFD (p-CMFD) which uses the partial currents instead of the net current was proposed [18]. Those analyses were performed with the specific transport methods excluding the DFEM-Sn. In this work, the p-CMFD method is analyzed and then improved for the application to the DFEM-Sn as an alternative to the regular CMFD. Its performance is also compared with that of the net current based CMFD.

In Section 3, the specifics of the CMFD formulation for DFEM-Sn are described starting from the methods for acquiring the coarse mesh average fluxes and net currents to construct the CMFD problem. The details of the alternating calculation scheme to exchange the updated information between the CMFD and DFEM-Sn methods are presented. The weakness of the original p-CMFD method is then identified and the modified p-CMFD method is proposed by correcting the deficiency of the original p-CMFD method.

In Section 4, three different CMFD methods, namely, CMFD, p-CMFD and modified p-CMFD are examined first for a set of 2-D test problems constructed by using three different materials of the C5G7MOX benchmark problem [23] to examine the performance and stability of these acceleration methods. Different core sizes and coarse mesh sizes are examined. The effectiveness of the CMFD acceleration is then assessed for the 3D problems such as the IAEA3D (International Atomic Energy Agency Three-Dimensional) problem [24] and the C5G7MOX benchmark problems [23]. Section 5 concludes the paper.

2. DISCONTINUOUS FINITE ELEMENT METHOD FORMULATION OF FEDONA

DFEM is to take the advantage of solving small linear systems constructed for each element instead of solving the large linear system constructed for the global problem. The small linear system built for a tetrahedron element is solved in the element-by-element fashion to determine the solution for the entire problem. The order of element sweep is thus essential for each discrete angle of the Sn equation. This sweeping order should be predetermined before solving the linear systems by considering the relation between the discrete angle and the element surface. The determination of the sweeping order is described at the end of the following section which provides the DFEM formulation for the Sn equation. Since the DFEM calculation basically requires iterations, a proper control of various iteration levels to update fission and scattering sources and to terminate the sweeping is essential. In this regard, the residual reduction ratio is defined in Section 2.2 as the convergence parameter for the self-scattering source update iteration (the inner iteration) and the overall iteration control logic is provided. The FEDONA code system and the calculation procedure including the external mesh generation and post-processing utility are then explained in Section 2.3.

2.1 DFEM Spatial Discretization for Sn Equation

The conventional Sn equation with isotropic scattering is given as the following within-group transport equation for the m-th angular flux multiplied by 4π with the energy group index omitted:

$$\hat{\Omega}_m \cdot \nabla \varphi_m(\vec{r}) + \Sigma_t \varphi_m(\vec{r}) = \Sigma_s \phi(\vec{r}) + q(\vec{r}), \quad \vec{r} \in V \tag{1}$$

where Σ_t and Σ_s are the macroscopic total and scattering cross sections and $q(\vec{r})$ is the source term including fission and scattering from other groups. The scalar flux $\phi(\vec{r})$ is obtained as the weighted average of angular fluxes as follows with the given angular quadrature set $\{\hat{\Omega}_m, \omega_m\}_{1 \le m \le M}$:

$$\phi = \sum_{m=1}^{M} \omega_m \varphi_m \quad \text{and} \quad \sum_{m=1}^{M} \omega_m = 1. \tag{2}$$

To apply the DFEM, the angular flux in element k is approximated as a linear combination of the basis functions of which the number is equal to the number of nodes (vertices of the element). For the tetrahedral elements, there are always four nodes and thus the linear combination for the angular flux involves four basis functions. Each of the four basis functions vanishes at all the other nodes than the node of interest where the basis function becomes unity. By denoting the i-th basis function, which is for Node i, by $u_i^k(\mathbf{r})$ and the four element vectors consisting of the four node angular fluxes and the four basis functions by $\boldsymbol{\varphi}_m^k$, and $\mathbf{u}^k(\vec{r})$, respectively, the angular and scalar fluxes are represented as:

$$\varphi_m^k(\vec{r}) \cong (\boldsymbol{\varphi}_m^k)^T \mathbf{u}^k(\vec{r}) = \sum_{i=1}^{N} \varphi_{m,i}^k u_i^k(\vec{r}). \tag{3}$$

With this representation, the DFEM equation is derived by conducting a weighted integration of Eq. (1) with the j-th weighting function $v_j^k(\vec{r})$ as:

$$\begin{aligned} &\int_{V_k} dV v_j^k \hat{\Omega}_m \cdot \nabla \left((\boldsymbol{\varphi}_m^k)^T \mathbf{u}^k \right) + \int_{V_k} dV \Sigma_t (\boldsymbol{\varphi}_m^k)^T \mathbf{u}^k v_j^k \\ &= \int_{V_k} dV \Sigma_s (\boldsymbol{\phi}^k)^T \mathbf{u}^k v_j^k + \int_{V_k} dV v_j^k (\mathbf{q}^k)^T \mathbf{u}^k. \end{aligned} \tag{4}$$

By employing the divergence theorem to the first term of Eq. (4), the following is obtained:

$$\begin{aligned} &\sum_{s=1}^{N_s} \int_{\partial V_{k,s}} \hat{\Omega}_m \cdot \hat{n}_k^s (\boldsymbol{\varphi}_m^k)^T \mathbf{u}^k v_j^k dA - \int_{V_k} \left(\hat{\Omega}_m \cdot \nabla v_j^k \right) (\boldsymbol{\varphi}_m^k)^T \mathbf{u}^k dV \\ &+ \int_{V_k} \Sigma_t (\boldsymbol{\varphi}_m^k)^T \mathbf{u}^k v_j^k dV = \int_{V_k} \Sigma_s (\boldsymbol{\phi}^k)^T \mathbf{u}^k v_j^k dV + \int_{V_k} v_j^k (\mathbf{q}^k)^T \mathbf{u}^k dV \end{aligned} \tag{5}$$

where s is the element surface index and $\hat{n}_k^s$ is the outward normal unit vector of surface s. In the DFEM-Sn, the leakage through a surface of the element is separated into the outgoing and incoming angular flux terms as follows:

$$\varphi_m^{k,s}(\vec{r}) = \begin{cases} (\boldsymbol{\varphi}_m^{k,out})^T \mathbf{u}^k(\vec{r}), & \hat{n}_k^s \cdot \hat{\Omega}_m > 0 \\ (\boldsymbol{\varphi}_m^{k',in})^T \mathbf{u}^{k'}(\vec{r}), & \hat{n}_k^s \cdot \hat{\Omega}_m < 0 \end{cases} \tag{6}$$

where k' is the index of the neighboring element which provides the incoming angular flux to element k. Note that this is caused by the discontinuity of the angular flux at each element node since the updated angular fluxes for element k are calculated with the outgoing node angular fluxes of incoming side neighboring element k', and these become the incoming angular flux sources of the outgoing side neighboring element.

With this discontinuous choice, Eq. (5) can be rewritten as the following by moving the incoming side streaming term to the right hand side:

$$\begin{aligned} &\sum_{s=1}^{N_{out}} \int_{\partial V_{k,s}} \left| \hat{\Omega}_m \cdot \hat{n}_k^s \right| (\boldsymbol{\varphi}_{m,k}^{out})^T \mathbf{u}^k v_j^k dA - \hat{\Omega}_m \cdot \int_{V_k} \left(\nabla v_j^k \right) (\boldsymbol{\varphi}_m^k)^T \mathbf{u}^k dV \\ &+ \int_{V_k} \Sigma_t (\boldsymbol{\varphi}_m^k)^T \mathbf{u}^k v_j^k dV = \sum_{s=1}^{N_{in}} \int_{\partial V_{k,s}} \left| \hat{\Omega}_m \cdot \hat{n}_k^s \right| (\boldsymbol{\varphi}_{m,k'}^{in})^T \mathbf{u}^k v_j^k dA \\ &+ \int_{V_k} \Sigma_s (\boldsymbol{\phi}^k)^T \mathbf{u}^k v_j^k dV + \int_{V_k} v_j^k (\mathbf{q}^k)^T \mathbf{u}^k dV \end{aligned} \tag{7}$$

This is a weighted balance equation obtained with the weighting function $v_j^k(\vec{r})$ that contains four unknowns. In order to determine the four unknowns, four weighting functions need to be chosen to form different weighted balance equations of Eq. (7). By the Galerkin weighting scheme which is to choose the weighting function to be the same as the basis function, namely, $v_j^k(\vec{r}) = u_j^k(\vec{r})$, the following linear system is obtained for each element:

$$\left[\sum_{s=1}^{N_{out}} \mathbf{L}_{m,k}^{s,out} + \mathbf{O}_m^k + \Sigma_t \mathbf{F}_k \right] \boldsymbol{\varphi}_m^k = \mathbf{F}_k \left(\Sigma_s \boldsymbol{\phi}^k + \mathbf{q}^k \right) + \sum_{s=1}^{N_{in}} \mathbf{L}_{m,k'}^{s,in} \boldsymbol{\varphi}_m^{k'} \tag{8}$$

where

$$\begin{aligned} &(\mathbf{O}_m^k)_{ij} = -\int_{V_k} (\Omega_m^x \frac{\partial u_i^k}{\partial x} + \Omega_m^y \frac{\partial u_i^k}{\partial y}) u_j dV, \ (\mathbf{F}_k)_{ij} \\ &= \int_{V_k} u_i^k u_j^k dV, \ (\mathbf{L}_{m,k}^l)_{ij} = \int_{\partial V_{k,s}} |\hat{\Omega}_m \cdot \hat{n}_k^s| u_i^k u_j^k dA. \end{aligned} \tag{9}$$

This DFEM-Sn governing equation for element k is converted to the equation for the orthogonal local element coordinate system as in the standard FEM solution approach. The converted elementwise equation is then solved following the predetermined element sweeping order for angle m to produce the node angular and scalar fluxes. The element volume average scalar flux for the tetrahedral element is now obtained using the node scalar fluxes as follows:

$$\bar{\phi}^k = \frac{\int_{V_k} \phi(x,y,z) dV}{\int_{V_k} dV} = \frac{|J| \int_0^1 \int_0^{1-\zeta} \int_0^{1-\eta-\zeta} \sum_{i=1}^{4} \phi_i^k \hat{u}_i d\xi d\eta d\zeta}{|J| \int_0^1 \int_0^{1-\zeta} \int_0^{1-\eta-\zeta} d\xi d\eta d\zeta} = \frac{1}{4} \sum_{i=1}^{4} \phi_i^k \tag{10}$$

where J is the Jacobian matrix to transform the global coordinate system to the local element base coordinate system.

Before performing the DFEM-Sn calculation employing the above equation, the FEDONA code prepares the element sweeping order for each discrete angle so that the solution process becomes a simple element-by-element calculation of the small linear system following this order. The tetrahedron elements are classified into three types according to the

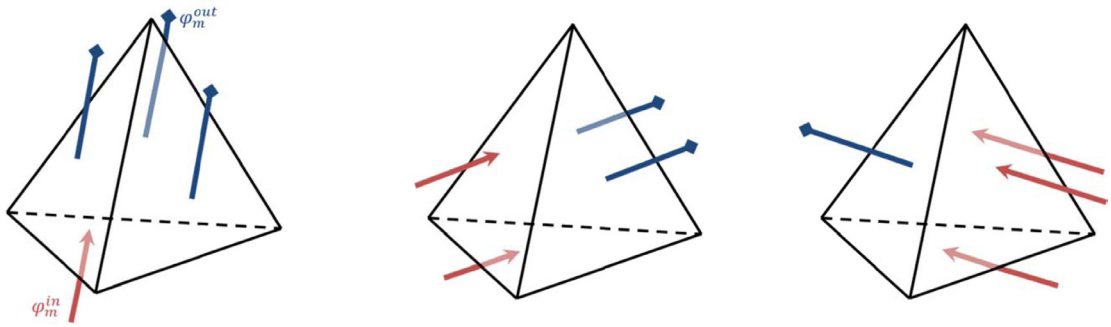

(a) 1 in / 3 out (b) 2 in / 2 out (c) 3 in / 1 out

Fig. 1. Types of Tetrahedral Elements

relation between the incoming angle and surfaces as illustrated in Fig. 1. The major principle of determining the sweeping order is to give priority to the element which has all the incoming angular fluxes from neighbor elements for the designated angle. Therefore, the sweeping order determination process starts from the boundary elements where the incoming angular fluxes are given from the boundary condition. The process finds in sequence an element satisfying the required number of incoming angular fluxes.

2.2 Residual Reduction Ratio for Inner Iteration Termination

Normally, in the iteration scheme of the DFEM-Sn calculation, the fission source iteration or the outer iteration is conducted by the power method, which is to update the fission sources and the eigenvalue after all the energy group fluxes are updated. On the contrary, the self-scattering source is updated by the flux of each energy group. The convergence of the self-scattering source iteration, namely the inner iteration, is considered to be more significant in the DFEM because the node angular fluxes at a node are not continuous and several iterations are necessary for the difference to diminish below a certain level. In this regard, a proper inner iteration convergence criterion is necessary in the iterative DFEM-Sn calculation to assure stable and efficient convergence. Based on the consideration that the total error of the whole problem domain is obtained by the summation of the element residuals which are defined for Eq. (8) as follows:

$$\begin{aligned}\tilde{r}_k(o,i) &= \Sigma_s \mathbf{M}_k \boldsymbol{\phi}^{k(o,i)} + \mathbf{Q}^{k(o-1,0)} \\ &+ \sum_{m=M_1}^{M_n} \omega_m \left\{ \sum_{s=1}^{N_{in}} \mathbf{U}_{m,k}^{s,in} \boldsymbol{\varphi}_m^{k'(o,i-1/2)} \right. \\ &\left. - \left(\sum_{s=1}^{N_{out}} \mathbf{U}_{m,k}^{s,out} + \mathbf{K}_m^k + \Sigma_t \mathbf{M}_k \right) \boldsymbol{\varphi}_m^{k(o,i)} \right\}\end{aligned} \tag{11}$$

where the (o, i) pair denotes the o-th outer and i-th inner iteration step, respectively. The norm of the volume weighted global residual vector is used for monitoring error reduction. Specifically, the total residual for the (o, i) step is determined as:

$$R_{err}(o,i) = \sqrt{\sum_{k=k_1}^{k_N} \left(\tilde{r}_k(o,i) V_k \right)^2} = \left\| \mathbf{V}\tilde{\mathbf{r}}(o,i) \right\| \tag{12}$$

where the diagonal matrix $\mathbf{V}$ consists of the element volumes. The residual reduction ratio is then defined as the ratio of the total residual of the present inner iteration step to that obtained before the first inner iteration, namely,

$$r_{err}^i = \frac{R_{err}(o,i)}{R_{err}(o,0)}. \tag{13}$$

The residual reduction ratio decreases as the self-scattering iteration proceeds but shows different behaviors for each group according to the magnitude of the scattering ratio.

2.3 The FEDONA code system

In order to perform the DFEM calculations for a general geometry, mesh generation should be performed first outside the FEDONA code. The mesh generation in the FEDONA code system is done by a public mesh generation utility Gmsh which takes the problem geometry description generated by using a computer aided design software such as CATIA. The information about the tetrahedron elements generated by Gmsh that is consisted of the node and element data is then processed by the GENI code to generate the surface information and to assemble all the elements data into the FEDONA input format. The geometry data are read in FEDONA along with the cross section data and problem parameters. After finishing the DFEM-Sn calculation in FEDONA, the element-wise flux and power distribution information is produced in a special file format for post-processing visualization by the VisIt [25] package. Fig. 2 shows the entire FEDONA code system.

FEDONA has parallel computing capability based on the OpenMP parallelization package. Parallelization is done on

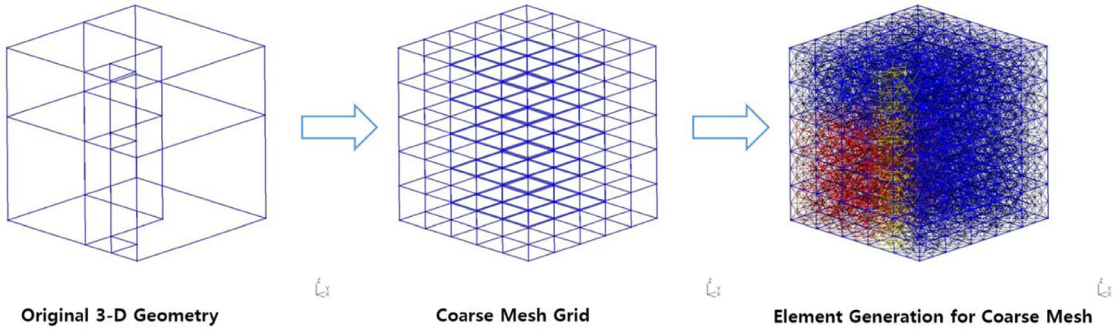

Fig. 3. Coarse Mesh Grid and Finite Element Generation for CMFD Calculation

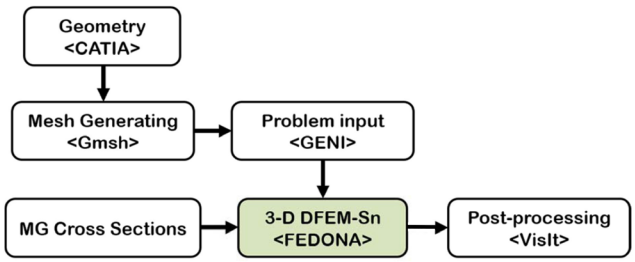

Fig. 2. The FEDONA Code System

the basis of angular decomposition so that parallel computations are done for a group of discrete angles formed by noting that the angles mutually related by the reflective boundary condition should belong to the same group. A processing thread is assigned to each reflective angular group and thus three threads are assigned to S_4 calculations.

3. CMFD FORMULATION FOR DFEM-SN

The CMFD correlation between the net current and average fluxes in a two coarse mesh configuration containing an interfacial surface is constructed using the information available from the high order transport method. This correlation is used in the CMFD problem which is to determine the globally balanced coarse mesh-wise flux and fission source distributions. The remarkable effectiveness of CMFD is attained owing to its ability to converge the global coarse meshwise fission source distribution rapidly [11]. For the actual implementation of the CMFD acceleration, an efficient linear system solver is necessary to determine the 3-D coarse mesh flux distribution effectively. In FEDONA, the BiCGSTAB method employing the BILU3D preconditioner [26] is used.

Normally, regular rectangular geometries are used in the CMFD method, whereas irregular tetrahedron meshes are used in the DFEM-Sn calculation. Thus, it is necessary to form a rectangular grid structure for the CMFD meshes first before generating the tetrahedral elements as illustrated in Fig. 3. With the tetrahedral elements whose surfaces are aligned with the rectangular coarse mesh surfaces, the coarse mesh average fluxes and the net current at the coarse mesh interface can be readily obtained as described in section 3.1. It should be noted, however, that the work here is targeted for the rectangular CMFD meshes for the proof-of-principle demonstration of the CMFD acceleration of DFEM-Sn calculations. In general, non-orthogonal geometries can be used in the CMFD calculation.

In the following section, the CMFD formulation for DFEM-Sn is derived first by using the net current. The scheme for alternating calculations between the CMFD and DFEM-Sn problems, that involve the restriction and prolongation operations on the fluxes, is also presented in Section 3.2. Lastly, the modified formulation of the p-CMFD is proposed in Section 3.3.

3.1 Generation of CMFD Parameters from Sn Transport Solution

The current correction coefficient $\hat{D}$ is employed in the following CMFD relation between the net current at the interface and the two coarse mesh average fluxes:

$$J_{c+1/2} = -\tilde{D}_{c+1/2}\left(\phi_{c+1} - \phi_c\right) + \hat{D}_{c+1/2}\left(\phi_{c+1} + \phi_c\right) \tag{14}$$

where the index *c+1/2* designates the surface between the *c*-th and *(c+1)*-th coarse meshes and $\tilde{D}$ is the finite difference method-based current coefficient which is solely determined by the inverse of transport cross sections and sizes of the two meshes as:

$$\tilde{D}_{c+1/2} = \frac{2\beta_c\beta_{c+1}}{\beta_c + \beta_{c+1}} \tag{15}$$

with $\beta_c = \frac{D_c}{h_c}$. Here the coarse mesh average flux for mesh *c* is obtained by element volume weighting such as:

$$\phi_c = \frac{1}{V_c}\sum_{V_k \in V_c} V_k \phi_k^c \quad . \tag{16}$$

The current correction coefficient $\hat{D}$ is defined by the coarse mesh surface current $J_{c+1/2}$ which is obtained from the angular fluxes of the nodes residing on the coarse mesh surface as:

$$\hat{D}_{c+1/2} = \frac{J_{c+1/2} + \tilde{D}_{c+1/2}\left(\phi_{c+1} - \phi_c\right)}{\phi_{c+1} + \phi_c}. \tag{17}$$

When determining the net current on the coarse mesh surface, it should be noted that the node angular fluxes are not continuous in the DFEM calculation and the number of available different angular fluxes at each node is the same as that of elements sharing the node. Since only one current should be used in determining the net surface current of Eq. (14), it is necessary to formulate an appropriate method to construct the net current.

Now, consider the two elements sharing a surface *c+1/2* shown in Fig. 4. The blue element is located in the *c-th* coarse mesh, while the red element is in the (*c+1*)-th coarse mesh. Although the shapes of the two elements shown in the left side of the figure look slightly different from those of shown on the right, they represent the same pair of elements. For the blue element on the left, the incoming partial current denoted by J_{in} should be determined by the angular fluxes of the three nodes of the red element on the right. Note that each node is marked with two colors to designate that there are two node values. On the other hand, the outgoing partial current should be determined by the values of the blue element. With δ_m being the projection of direction *m* to the outward normal vector of the interfacing surface, the partial currents at the element node are given as:

$$J^{k,out}_{c+1/2} = \sum_{m=1}^{M/2} \delta_m \omega_m \varphi^k_{m,i} \quad , \quad J^{k',out}_{c+1/2} = \sum_{m=M/2+1}^{M} \delta_m \omega_m \varphi^{k'}_{m,i} \tag{18}$$

where *k* and *k'* are the indices of the blue and red elements, respectively. Since there are three nodes on the triangular interface of a tetrahedral element, the element surface net current is determined by taking the average of the partial currents of the three nodes as follows:

$$J^{k,net}_{c+1/2} = \frac{1}{3}\sum_{i=1}^{3}\left(J^{k,out}_{c+1/2} - J^{k',out}_{c+1/2}\right). \tag{19}$$

Here the outgoing partial currents of each element are selected because these become the transferring incoming flow term in DFEM as shown in Eq. (8). Since there are several elements contacting a coarse mesh surface, the net current on the coarse mesh surface is obtained by accounting for the element surface area ratio as:

$$J_s = \sum_{k=1}^{K_s} \rho^k_s J^{k,net}_s, \quad \rho^k_s = \frac{A^k_s}{A^c_s}, \quad s = c+1/2 \tag{20}$$

where A^k_s is the area of surface s for element *k* and A^c_s is the area of the coarse mesh surface.

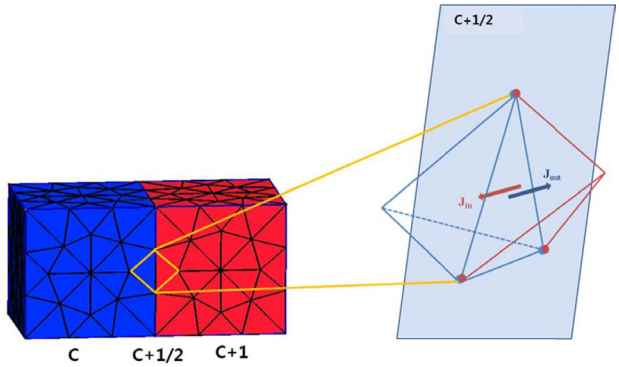

Fig. 4. Partial Currents on the Element Surface between Two Coarse Meshes

3.2 Alternating Calculations between CMFD and DFEM-Sn

After each CMFD calculation, the updated coarse mesh average flux and eigenvalue should be fed back to the subsequent DFEM-Sn calculation to construct the node wise source. In contrast to constructing the coarse mesh average flux which is a restriction process, a prolongation process is necessary to update the scalar fluxes of the elements and nodes using the coarse mesh values. This is done by using the flux ratios determined in the previous DFEM-Sn calculations as follow:

$$\phi^{(l)}_k = \left(\frac{\phi^{(l-1)}_k}{\phi^{(l-1)}_{c,Sn}}\right)\cdot\phi^{(l)}_{c,CMFD} \quad , \quad \phi^{(l)}_{k,i} = \left(\frac{\phi^{(l-1)}_{k,i}}{\phi^{(l-1)}_k}\right)\cdot\phi^{(l)}_k \tag{21}$$

where

$\phi^{(l-1)}_{c,Sn}$ = coarse mesh cell average flux determined at the (*l*-1)-th Sn calculation

$\phi^{(l)}_{c,CMFD}$ = coarse mesh cell average flux determined at the *l*-th CMFD calculation

$\phi^{(l)}_k$ = element average flux at the *l*-th step

$\phi^{(l)}_{k,i}$ = *i*-th node scalar flux of element *k* at the *l*-th step.

Particularly for the reflective boundary surface, the node angular fluxes should be reconstructed as well for the initial incoming angular flux term. This is done by using the ratio of the incoming partial currents and the node angular fluxes as follows:

$$\varphi^{(l)}_{m,k,i} = \left(\frac{J^{(l)}_{in,CMFD}}{J^{(l-1)}_{in,Sn}}\right)\cdot\varphi^{(l-1)}_{m,k,i}$$
$$J^{CMFD}_{in} = \frac{1}{4}\phi^s_c - \frac{1}{2}J_{net} = \frac{1}{4}\phi^s_c \quad \left(\because J_{net} = 0\right) \tag{22}$$

where

$J^{(l-1)}_{in,Sn}$ = incoming partial current determined at the (*l*-1)-th Sn calculation

$J^{(l)}_{in,CMFD}$ = incoming partial current, determined at the *l*-th CMFD calculation

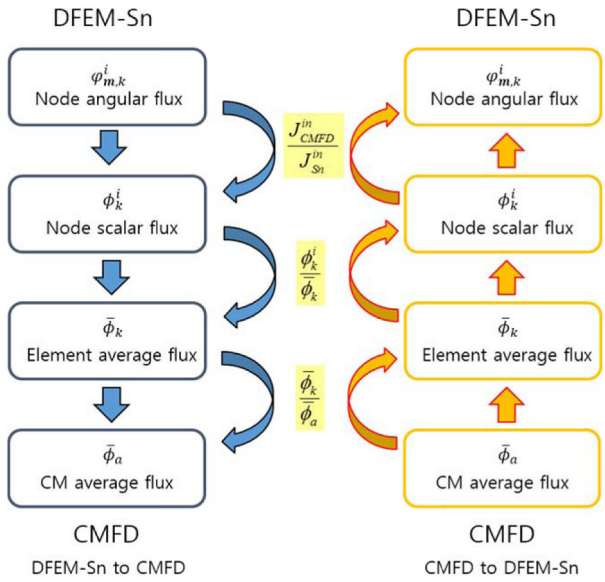

Fig. 5. Alternating CMFD and DFEM-Sn Calculation Scheme

ϕ_c^s = average surface flux of coarse mesh cell c.

The updated element average fluxes, node scalar fluxes, and node angular fluxes are used to construct the source terms in the right hand side of Eq. (8) to perform the next DFEM-Sn calculation. The step-by-step CMFD/DFEM-Sn calculation flow is illustrated in Fig. 5.

3.3 p-CMFD and Modified p-CMFD Formulation

Partial currents are necessary for constructing the coarse mesh net current because of the inherent discontinuity of the angular fluxes in the DFEM-Sn calculation. It is also reported that p-CMFD is more effective in larger mesh applications [20]. Therefore, it is worth examining the partial current-based CMFD formulation to accelerate the DFEM-Sn calculations.

The p-CMFD formulation differs from the standard CMFD only in the treatment of the current correction term. Specifically, the partial currents are represented as the following form in terms of the partial current correction coefficients defined for both directional partial currents:

$$\begin{aligned} J^+_{c+1/2} &= -\frac{1}{2}\tilde{D}_{c+1/2}\left(\phi_{c+1}-\phi_c\right)+\hat{D}^+_{c+1/2}\phi_c \\ J^-_{c+1/2} &= \frac{1}{2}\tilde{D}_{c+1/2}\left(\phi_{c+1}-\phi_c\right)+\hat{D}^-_{c+1/2}\phi_{c+1} \end{aligned} \tag{23}$$

where $\tilde{D}_{c+1/2}$ is defined in Eq.(15). These relations lead to the following partial current correction coefficients:

$$\begin{aligned} \hat{D}^+_{i+1/2} &= \frac{2J^+_{i+1/2}+\tilde{D}_{i+1/2}\left(\phi_{i+1}-\phi_i\right)}{2\phi_i} \\ \hat{D}^-_{i+1/2} &= \frac{2J^-_{i+1/2}-\tilde{D}_{i+1/2}\left(\phi_{i+1}-\phi_i\right)}{2\phi_{i+1}} \end{aligned} \tag{24}$$

The partial currents to be used in these formulas are those obtained by Eq. (18). For the vacuum boundary condition, the boundary partial currents are described as the following which is given for the 1-D slab geometry having nodes from 1 to N as an example:

$$\begin{aligned} &\text{(left side)} \quad J^-_{1-1/2} = \frac{1}{2}\tilde{D}_{1-1/2}\phi_1+\hat{D}^-_{1-1/2}\phi_1 \quad , \quad J^+_{1-1/2}=0 \\ &\text{(right side)} \quad J^+_{N+1/2} = \frac{1}{2}\tilde{D}_{N+1/2}\phi_N+\hat{D}^+_{N+1/2}\phi_N \; , \; J^-_{N+1/2}=0 \end{aligned} \tag{25}$$

In comparison to the standard CMFD relation given in Eq. (14), Eq. (23) takes merely half of the correction term in. Accordingly, the correction coefficients of the two CMFD relations satisfy the following relation:

$$\hat{D}_{c+1/2} = \frac{\hat{D}^-_{c+1/2}\phi_{c+1}-\hat{D}^+_{c+1/2}\phi_c}{\phi_{c+1}+\phi_c}. \tag{26}$$

The use of the partial current correction coefficients in the p-CMFD formulation would yield a different linear system from the one resulting from the standard CMFD formulation.

However, it is noted that the representation of the partial currents by Eq. (23) does not include the contribution from the flux itself, which can be the dominant term in determining the magnitude of the partial current. Note, that the most fundamental form of the partial current can be obtained by employing the P1 approximation and the finite difference approximation as:

$$\begin{aligned} J^+_{c+1/2} &= \frac{1}{4}\phi_{c+1/2}+\frac{1}{2}J_{c+1/2} \\ &= \frac{1}{4}\left(\omega_c\phi_c+(1-\omega_c)\phi_{c+1}\right)-\frac{1}{2}\tilde{D}_{c+1/2}\left(\phi_{c+1}-\phi_c\right). \end{aligned} \tag{27}$$

where $\omega_c = \frac{\beta_c}{\beta_c+\beta_{c+1}}$. Considering the surface flux term $\phi_{c+1/2}$ which is obtained as the weighted average of the two mesh average fluxes, the p-CMFD formulation can be modified as follows:

$$\begin{aligned} J^+_{c+1/2} &= \frac{1}{4}\left(\omega_c\phi_c+(1-\omega_c)\phi_{c+1}\right) \\ &\quad -\frac{1}{2}\tilde{D}_{c+1/2}\left(\phi_{c+1}-\phi_c\right)+\hat{\hat{D}}^+_{c+1/2}\phi_c \\ J^-_{c+1/2} &= \frac{1}{4}\left(\omega_c\phi_c+(1-\omega_c)\phi_{c+1}\right) \\ &\quad +\frac{1}{2}\tilde{D}_{c+1/2}\left(\phi_{c+1}-\phi_c\right)+\hat{\hat{D}}^-_{c+1/2}\phi_{c+1} \end{aligned} \tag{28}$$

by introducing different correction coefficients $\hat{\hat{D}}^+_{c+1/2}$ and $\hat{\hat{D}}^-_{c+1/2}$.

Eq. (28) can also be used in the standard CMFD equation by subtracting the incoming from the outgoing partial current which would cancel the surface flux term. It

is noted, however, that the two current correction coefficients are retained on each surface by Eq. (28), whereas there is only one current correction coefficient in the standard CMFD formulation. These new current correction coefficients $\hat{\tilde{D}}^{\pm}_{c+1/2}$ would lead to a different convergence performance. Note, that the vacuum boundary conditions for partial currents at both ends are now represented as:

$$\begin{aligned} &\text{(left)} \quad J^{-}_{1-1/2} = \left(\frac{1}{4}+\frac{1}{2}\tilde{D}_{1-1/2}+\hat{\tilde{D}}^{-}_{1-1/2}\right)\phi_1 \quad , \quad J^{+}_{1-1/2}=0 \\ &\text{(right)} \quad J^{+}_{N+1/2} = \left(\frac{1}{4}+\frac{1}{2}\tilde{D}_{N+1/2}+\hat{\tilde{D}}^{+}_{N+1/2}\right)\phi_N \, , \, J^{-}_{N+1/2}=0 \end{aligned} \tag{29}$$

which are obtained by taking the flux beyond the physical core to be zero in Eq. (28).

4. PERFORMANCE EXAMINATION

The performance of the CMFD acceleration of any transport calculations can be assessed first by the reduction in the number of transport sweeps. The extent of reduction can be dependent on the problem (or core) size, the size of the coarse meshes chosen, and the specifics of the CMFD formulation. In this regard, a set of 2-D eigenvalue problems are constructed to examine the dependence of three CMFD formulations of the DFEM-Sn on the problem and coarse mesh sizes. The multigroup cross sections taken from the C5G7MOX benchmark problem [23] consisting of UO_2 and MOX fuels and water reflector are used in the test problems. In the actual modeling of the 2-D problems with tetrahedron elements, a 3-D configuration for a slice of the reactor is used with the reflective boundary condition being applied at the top and bottom surfaces. The radial size of the core is varied from the smallest core of a 3x3 array of assemblies in a quarter core configuration to the largest core of 9x9 array of assemblies as illustrated in Fig. 6. The 5x5 and 7x7 arrays are added so that there are a total of four problems. Three different coarse mesh sizes, namely, one sixteenth of an assembly mesh, a quarter and the entire assembly size, are examined. The performance of the p-CMFD and modified p-CMFD are examined along with the standard CMFD. The S_4 angular quadrature set is used in all these calculations. One Sn transport sweep is performed per the DFEM-Sn update before proceeding to the subsequent CMFD (or p-CMFD) calculation by default. But more transports sweeps are invoked if instability is detected for larger coarse mesh problems. The criterion for the residual reduction ratio to exit the inner iteration is set to 10^{-4} for sufficient convergence of the in-group calculations. The convergence criteria for the eigenvalue and the relative global fission source error are set to 10^{-6} and 10^{-4}, respectively. In the following, the CMFD performance is examined first for the 2-D test problems and then for the 3-D benchmark problems consisting of the IAEA [24] and the C5G7MOX problems.

4.1 CMFD Performance for 2-D Test Problems

The four 2-D problems are illustrated in Fig. 7 with the widths of the core and the number of tetrahedral elements used. The maximum coarse mesh width is 21.42 cm, while the smallest is 5.355 cm. The base coarse mesh size is set to 5.355 cm and the elements were generated with the basic coarse mesh structure so that the element configuration need not be changed for the lager coarse mesh cases. Namely, the same element configuration is used for the 10.71 cm and 21.42 cm coarse mesh cases, which can be constructed by merely using the elements in the 2x2 or 4x4 basic meshes. The average element pitch is about 2.5cm. The results of the CMFD acceleration are presented in Table 1 with the number of DFEM-Sn transport sweeps for different problem and coarse mesh sizes. The p-CMFD and modified p-CMFD results are also given in the table. As shown in this table, the CMFD acceleration reduces the outer iterations by a factor of 1.7 through 27.3.

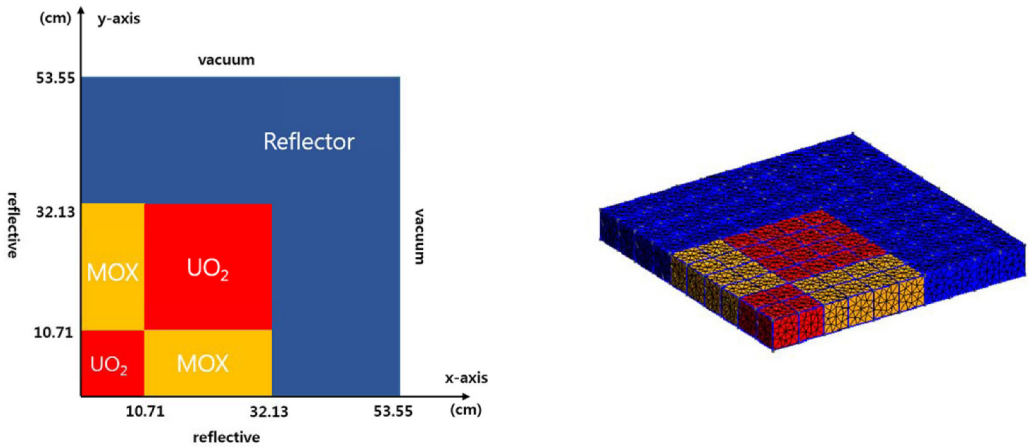

Fig. 6. Configuration of the 3x3 Test Problem

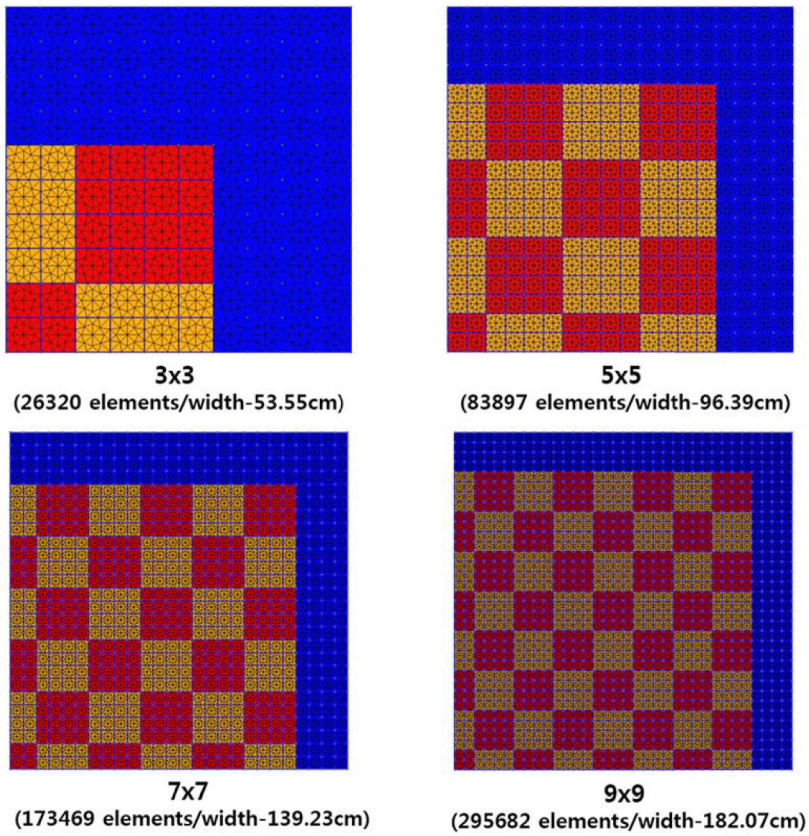

Fig. 7. Configuration of the 2-D Test Problem Set

Table 1. Number of Sn/CMFD Calculations for Different Problem and Coarse Mesh Sizes in 2-D Test Problems

Problem	Sn w/o CMFD	CM size (cm)	w/CMFD		w/mp-CMFD[a]		w/p-CMFD	
			Sn	CMFD	Sn	mp-CMFD	Sn	p-CMFD
3x3	22	5.355	7 (3.1)[b]	6	8 (2.8)	7	13 (1.7)	12
		10.71	13 (1.7)	12	14 (1.6)	13	17 (1.3)	16
		21.42	13 (1.7)	6	14 (1.6)	7	20 (1.1)	19
5x5	62	5.355	5 (12.4)	4	6 (10.3)	5	9 (6.9)	8
		10.71	9 (6.9)	8	9 (6.9)	8	12 (5.2)	11
		21.42	14 (4.4)	7	11 (5.6)	5	24 (2.6)	23
7x7	120	5.355	6 (20.0)	5	7 (17.1)	6	8 (15.0)	7
		10.71	9 (13.3)	8	11 (10.9)	10	12 (10.0)	11
		21.42	13 (9.2)	6	13 (9.2)	6	22 (5.5)	21
9x9	191	5.355	7 (27.3)	6	8 (23.9)	7	9(21.2)	8
		10.71	10 (19.1)	9	10 (19.1)	9	12 (15.9)	11
		21.42	13 (14.7)	6	15 (12.7)	7	18 (10.6)	17

[a] Modified p-CMFD method
[b] Reduction factor of Sn transport sweeps comparing to the Sn w/o CMFD outer iteration number

It is noted that the number of transport sweeps with the CMFD acceleration remains almost unchanged by the problem size, while it increases significantly if no acceleration is applied. It indicates the fact that the CMFD acceleration is much more effective for large problems having large dominance ratios. For the 9x9 quarter core problem, which has nearly the same radial size as a realistic core, the standard CMFD formulation reduces the number of transport sweeps to 7 from 191 of the ordinary DFEM-Sn calculation case. This significant reduction in the number of transport sweeps is possibly because the CMFD solution can provide fast converging global coarse mesh wise fission source distribution. The transport sweeps take the role of updating the local relations between the net current and coarse mesh average fluxes, and thus the number of transport sweeps does not significantly increase once the local configuration and properties are fixed as in the 2-D test problems.

Similar reduction is observed with p-CMFD and modified p-CMFD, although somewhat diminished efficiency is noted with the original p-CMFD for all the cases. The modified p-CMFD yields substantially notable performance improvement over the original p-CMFD, yet it shows slightly worse performance than the standard CMFD. The acceleration performance is more clearly compared in the error reduction plot given Fig. 8 which shows the fission source root mean square (RMS) errors of the 9x9 case. The reference fission source distribution used for this error estimation was generated by imposing a much tighter convergence condition so that the RMS fission source error defined below becomes nearly a true error:

$$\varepsilon_{RMS}^{(o)} = \sqrt{\sum_{k=1}^{K} \frac{\left(\psi_k^{(o)} - \psi_k^*\right)^2}{\psi_k^{(o)} \cdot \psi_k^*}} \qquad (30)$$

where $\psi_k^{(o)}$ is the normalized fission source of element k obtained at the o-th outer iteration step and ψ_k^* is the fission source of the tightly converged solution.

The number of transport sweeps given in Table 1 and the RMS error behavior of Fig. 8 indicate that the CMFD performance becomes diminished as coarse mesh size increases irrespective of the details of the CMFD formulation. This trend is an obvious consequence of the increased optical thickness with the larger coarse meshes. As shown in Table 2, that shows the optical thicknesses for the three materials of the C5G7MOX problem with the coarse mesh size of 10.71 cm, the optical lengths for the thermal energy group is higher than 10 and thus the spectral radius of the CMFD acceleration will be large. This leads to a deterioration of the convergence behavior in this seven-group problem if the chosen coarse mesh size is too large. The increase in the number of Sn sweeps observed for the 21.42 cm coarse mesh case is the obvious drawback of the increased optical thickness.

In general, there is no need to choose the coarse mesh size as large as possible in the CMFD acceleration of transport problems, because the computing time for the CMFD calculation is negligible compared to the transport calculation time. In these 2-D examples, the CMFD computing time is less than 1% of the total time even for the smallest coarse mesh size of 5.355cm. Therefore, it is preferred to keep the coarse mesh size sufficiently small so that the number of transport sweeps can be minimized and stable convergence can be achieved.

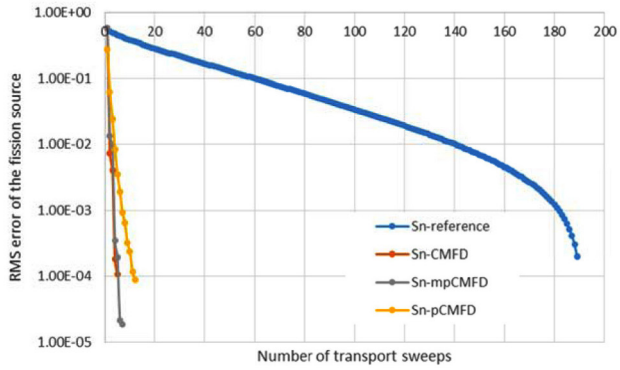

(a) CM size = 5.355cm

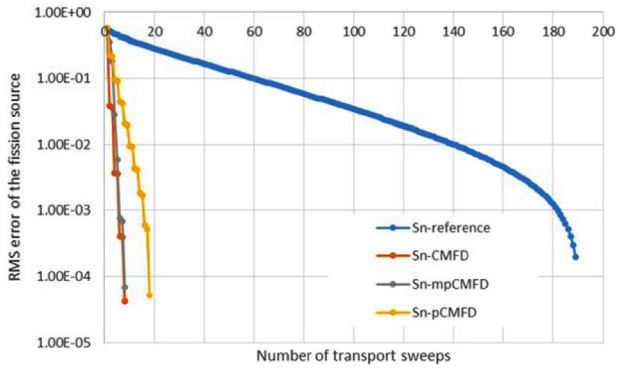

(b) CM size = 10.71cm

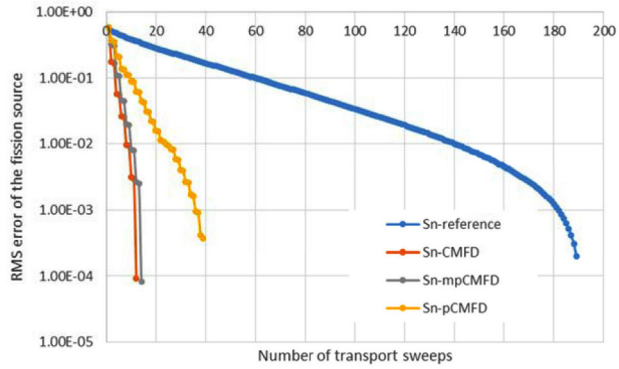

(c) CM size = 21.42cm

Fig. 8. Comparison of the Fission Source Error Reduction with the 9x9 Test Problem

Table 2. Optical Thickness ($\sum h$) of the 2-D problems for 10.71 cm Coarse Mesh

Group	Material		
	UO2	MOX	Ref.
1	1.79	1.81	1.71
2	3.90	3.92	4.42
3	5.56	5.63	6.32
4	5.93	6.12	6.26
5	5.27	6.18	7.69
6	8.47	10.91	13.44
7	16.98	19.01	28.39

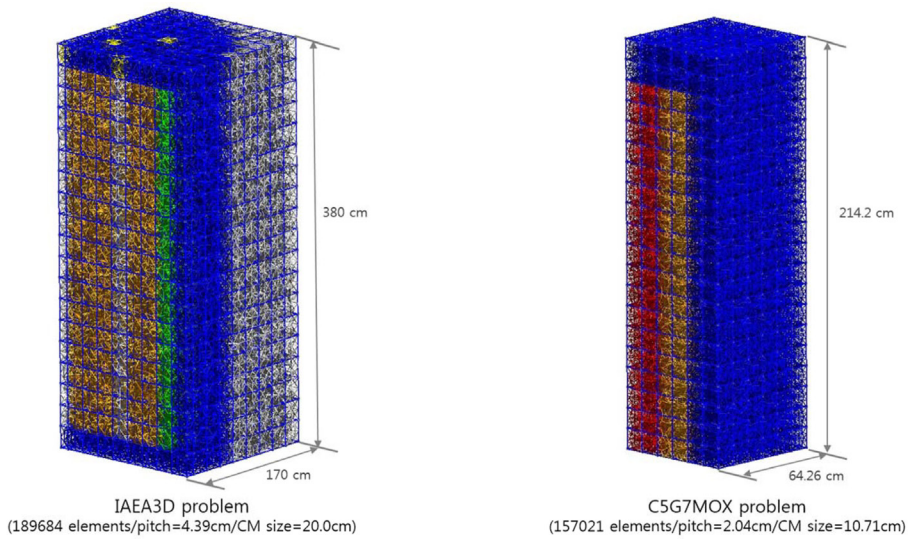

Fig. 9. 3-D Benchmark Problems with Tetrahedron Meshes

Table 3. Tetrahedron Elements Data for Benchmark Problems

Benchmark identification	Number of surfaces	Number of elements	Avg. element volume (cm^3)	Element pitch (cm)
IAEA3D	720792	189684	62.03	4.39
C5G7MOX	581716	157021	6.25	2.04

4.2 Verification of the CMFD Effectiveness with 3-D Benchmark Problems

The CMFD acceleration is now examined for the realistic 3-D benchmark problems. The first problem is the IAEA benchmark problem representing a typical light water reactor with two-group cross sections. The second one is the C5G7MOX benchmark problem with assembly homogenized seven-group cross sections. These cross sections were generated from a set of lattice transport calculations for the heterogeneous assemblies. The detailed configuration of the problems and the element structure are shown in Fig. 9. The coarse mesh size of IAEA problem is 20.0cm. This seemingly large coarse mesh size is chosen because it is a two-group problem in which the optical length can not be so large even for the thermal group. For the C5G7MOX problem, the coarse mesh size is chosen to be 10.71 cm. The data for finite elements including the number of elements, surfaces, element pitch and volume is given in Table 3 for the two benchmark problems. Parallel computation was performed for these 3-D problems with

Table 4. Verification of the CMFD Performance for 3-D Benchmark Problems

Benchmark identification	Acceleration method	Number of iterations[a]	Computing time (sec)[b]	Reduction factor	k-eff
IAEA 3D (CM size = 20.0cm)	None (Sn only)	175	447788	--	1.029868
	CMFD	9 (19.4)	21133	21.2	1.029869
	p-CMFD	31 (5.6)	76977	5.8	1.029869
	mp-CMFD	11 (15.9)	25159	17.8	1.029869
C5G7MOX (CM size = 10.71cm)	None (Sn only)	84	182476	--	1.183606
	CMFD	8 (10.5)	19212	9.5	1.183606
	p-CMFD	26 (3.2)	55301	3.3	1.183606
	mp-CMFD	8 (10.5)	19578	9.3	1.183607

[a] Number of Sn transport sweeps and iteration reduction factor within parenthesis
[b] 3 Threads on an Intel Xeon E5-2650 Linux cluster

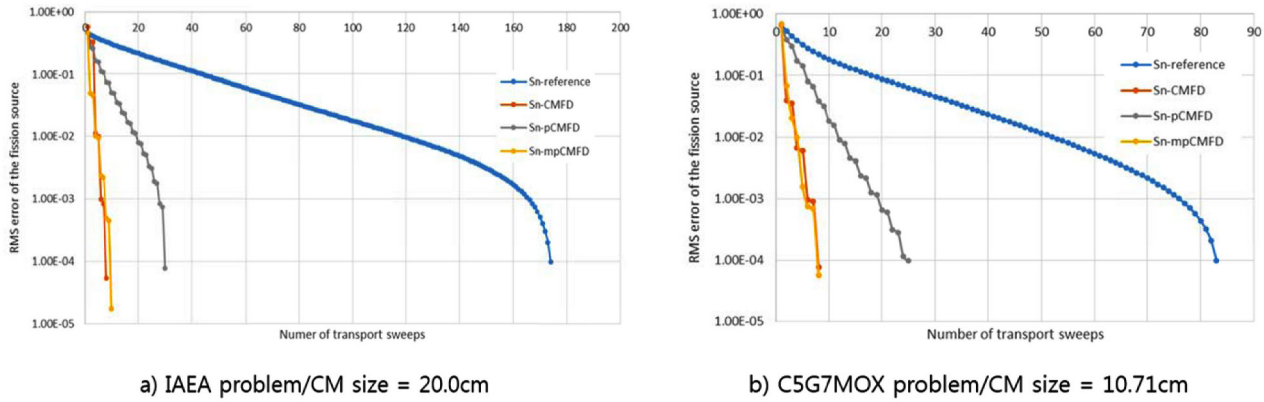

Fig. 10. Comparison of the Fission Source Error Reduction with 3-D Benchmark Problems

3 threads for the S_4 quadrature set. The number of outer iterations and computing times are given in Table 4 along with the acceleration factors.

In the IAEA benchmark, the CMFD acceleration reduces the number of iterations by a factor of 19.4 and the time reduction factor is 21.2. The reason for the slightly higher time reduction factor than the iteration reduction factor is attributed to the small error in the computing time measurement. The computing time reduction factor for the C5G7MOX problem is 9.5 which is smaller than the IAEA problem due to the smaller core size leading to a smaller dominance ratio. In both problems, the acceleration performance of the original p-CMFD formulation is poor, whereas the acceleration performance of the modified p-CMFD is comparable to the standard CMFD. The difference in the acceleration performance of the three CMFD formulations is clearly seen also in Fig. 10 that shows the fission source RMS error reduction.

5. CONCLUSIONS

As an effective acceleration method for the DFEM-Sn calculations for large reactor problems, the CMFD method was successfully applied and its superior performance was demonstrated. It was implemented into a 3-D DFEM-Sn code FEDONA which was developed for discrete ordinate neutron transport calculations in general geometries. The alternating DFEM-Sn and CMFD calculation scheme was established using the properly defined restriction and prolongation processes handling the element-wise and coarse mesh fluxes. A convergence check scheme employing the element-wise residual information was developed to properly terminate the within-group or inner iterations

As an alternative to the standard CMFD formulation, the partial current based CMFD formulation was also implemented and examined noting that the partial currents

have to be computed in determining the net current because of the inherent discontinuity in the node angular fluxes. It was found that it is better to add the surface flux term into the original p-CMFD expression for the partial current and mesh average fluxes, since the largest contribution to the partial current usually comes from the surface flux. The modified p-CMFD formulation that involves the surface flux term, however, shows merely comparable performance to the standard CMFD formulation although it is noticeably better than the original p-CMFD formulation.

As noted in the other CMFD accelerations of the reactor transport problems, the effectiveness of the CMFD acceleration of the DFEM-Sn calculation greatly increases with the core size due to the increasing dominance ratio of the large core problems. The number of DFEM-Sn transport sweeps remains almost unchanged with the increasing core size as demonstrated with the 2-D test problems. This is because the CMFD solution provides fast converging coarse mesh wise global fission source distributions, while a limited number of transport sweeps is sufficient to converge the local relations between the interface current and coarse mesh average fluxes.

Since the computing time for CMFD solutions is substantially shorter than the transport calculation time, and the convergence characteristics improve with the smaller coarse mesh sizes, it is desirable to use sufficiently small coarse mesh sizes such as one sixteenth of an assembly in the CMFD accelerated transport calculations. For the 3-D benchmark problems, the computing time reduction factor was as high as ~21 for the IAEA problem while it is ~9 for the C5G7MOX problem which is a much smaller problem than the IAEA problem.

Based on the verification results, it can be concluded that the standard CMFD formulation can effectively reduce the computing time of the DFEM-Sn calculations in large reactor eigenvalue problems. Since the CMFD acceleration can be applied to non-orthogonal geometries as long as the finite element surfaces lie on the coarse mesh surfaces, the CMFD method can be used for general geometry modeling.

ACKNOWLEDGEMENTS

This work was supported by the National Research Foundation of Korea (NRF) grant funded by the Korea government (MSIP) (No. 2013003535).

REFERENCES

[1] T.A. Wareing et al., "Discontinuous Finite Element SN Methods on Three-Dimensional Unstructured Grids," *Nucl. Sci. Eng.*, **138**, 256-268 (2001).

[2] J. M. McGhee, T.A. Wareing and D.A. Barnett Jr., *ATTILA User's Manual*, Transpire, Inc. (2007).

[3] S.G. Hong et al., "Development of MUST (Multi-group Unstructured geometry Sn Transport) Code," *Trans. of the Korean Nuclear Society*, Gyeongju, Korea (2009).

[4] W.H. Reed and T.R. Hill, *Triangular Mesh Methods for the Neutron Transport Equation*, Los Alamos Scientific Laboratory Report, LA-UR-83-479 (1973).

[5] B. Cockburn et al., "Discontinuous Galerkin Methods: Theory Computation and Applications," *Lecture Notes in Computational Science and Engineering*, **Vol. 11**, Springer-Verlag, New York, USA (2000).

[6] K.S. Smith, "Nodal method storage reduction by non-linear iteration," *Trans. of the American Nuclear Society*, **44**, 265 (1983).

[7] K.S. Smith and J.D. Rhodes III, "Full-core, 2-D, LWR core calculations with CASMO-4E," *Proc. of the ANS Reactor Physics Topical Meeting*, Seoul, Korea (2002).

[8] J.Y. Cho et al., "Cell based CMFD formulation for acceleration of whole-core method of characteristics calculation," *J. of the Korean Nuclear Society*, **34**, 250-258 (2002).

[9] Z. Zhong, T.J. Downar and Y. Xu, "Implementation of Two-Level Coarse-Mesh Finite Difference Acceleration in an Arbitrary Geometry, Two-Dimensional Discrete Ordinates Transport Method," *Nucl. Sci. Eng*, **158**, 289-298 (2008).

[10] K.S. Kim, M.D. DeHart, "Unstructured partial- and net-current based coarse mesh finite difference acceleration applied to the extended step characteristics method in NEWT," *Annals of Nuclear Energy*, **38**, 527-534 (2011).

[11] M.J. Lee, H. G. Joo, D. J. Lee and K. Smith, "Coarse mesh finite difference formulation for accelerated Monte Carlo eigenvalue calculation," *Annals of Nuclear Energy*, **65**, 101-113 (2014).

[12] H.G. Joo et al., "Dynamic implementation of the equivalence theory in the heterogeneous whole core transport calculation," *Proc of the ANS Reactor Physics Topical Meeting*, Seoul, Korea (2002).

[13] R.E. Alcouffe, "The Diffusion Synthetic Acceleration Methods for the Diamond-Differenced Discrete-Ordinates Equations," *Nucl. Sci. Eng.*, **64**, 344 (1997).

[14] E.W. Larsen, "Unconditionally Stable Diffusion Synthetic Acceleration Methods for the Slab Geometry Discrete Ordinates Equations. Part I: Theory," *Nucl. Sci. Eng.*, **82**, 47 (1982).

[15] M.L. Adams and W.R. Martin, "Diffusion Synthetic Acceleration of Discontinuous Finite Element Transport Iterations," *Nucl. Sci. Eng.*, **111**, 145 (1992).

[16] J.S. Warsa, T.A. Wareing and J.E. Morel, "Fully consistent diffusion synthetic acceleration of linear discontinuous SN transport discretizations on unstructured tetrahedral meshes," *Nucl. Sci. Eng.*, **141**, no.3, 236-251 (2002).

[17] J.S. Warsa, T.A. Wareing and J.E. Morel, "On the degraded effectiveness of diffusion synthetic acceleration for multidimensional Sn calculations in the presence of material discontinuities," *Proc. of Int. Conf. on Mathematics and Computational Methods Applied to Nuclear Science and Engineering*, Gatlinburg, TN, USA (2003).

[18] N.Z. Cho et al., "On a new acceleration method for 3D whole core transport calculations," *Proc. Annual Meeting of Atomic Energy Society of Japan*, Sasebo, Japan (2003).

[19] C. Geuzaine and J.F. Remacle, "Gmsh: a three dimensional finite element mesh generator with built-in pre and post processing facilities," *Int. Journal for Numerical Methods in Engineering*, **79**, Issue 11, 1309 (2009).

[20] N.Z. Cho and C.J. Park, "A Comparison of Coarse Mesh Rebalance and Coarse Mesh Finite Difference Accelerations

for the Neutron Transport Calculations," *Proc. of Int. Conf. on Mathematics and Computational Methods Applied to Nuclear Science and Engineering*, Gatlinburg, TN, USA (2003).
[21] A. Yamamoto et al., "Convergence Improvement of Coarse Mesh Rebalance Method for Neutron Transport Calculations," *J. of Nucl. Sci. Technol.*, **41**, 781-789 (2004).
[22] S.G. Hong, K.S. Kim and J.S. Song, "Fourier Convergence Analysis of the Rebalance Methods for Discrete Ordinates Transport Equations in Eigenvalue Problems," *Nucl. Sci. Eng.*, **164**, 33-52 (2010).
[23] E. Lewis et al., *Benchmark Specification for Deterministic 2-D/3-D MOX fuel Assembly Transport Calculations without Spatial Homogenization (C5G7MOX)*, NEA/NSC/DOC 4 (2001).
[24] Argonne Code Center, *Benchmark Problem Book*, Report ANL-7416 (Suppl. 2). Argonne National Laboratory, Argonne, IL (1977).
[25] LLNL, *VisIt User's Manual*, Lawrence Livermore National Laboratory Report, UCRL-SM-220449 (2005).
[26] H.G. Joo and T.J. Downar, "An incomplete domain decomposition preconditioning method for nonlinear nodal kinetics calculations," *Nucl. Sci. Eng.*, **123**, 403-414 (1996).